Journal of Engg. Research **Vol. 3 No. (3) September 2015** pp. 21-38

قدرة التحمل العمودي الغير مستنزف لكومة تقع بالقرب من منحدر طيني لين

محراب جسماني، *علي كسرانيا، ** مهراد كمال زارع و إيمان ميهديبور**

* قسم الهندسة المدنية، جامعة الإمام الخميني الدولية، قزوين، إيران

**قسم الهندسة المدنية والبيئية، معهد البوليتكنيك رينسيلار، تروي، وكلية مانهاتن، ريفرديل، ولاية نيويورك، الولايات المتحدة الأمريكية

*** قسم الهندسة المدنية، جامعة ميسوري للعلوم والتكنولوجيا، رولا، ولاية ميزوري، الولايات المتحدة الأمريكية

الخلاصـة

تم حساب قدرة تحمل الأسس الضحلة على منحدرات من مخططات التصميم المقترحة أو من خلال استخدام المعادلات التجريبية. يقدم هذا البحث نتائج دراسات العددية التي أجريت على سلوك كومة تقع بالقرب من منحدرات طينة لينة وتحت تأثير شروط سحب التحميل الرأسي الغير مستنزف. وتم إجراء سلسلة من النماذج العددية ثلاثية الأبعاد لمختلف أشكال كومات، مثل مسافات بين كومة وزاوية المنحدر. وأظهرت النتائج التي تم الحصول عليها، أنه كما زاد طول كومة، زادت معها امكانية تشكل الفشل الكامل لإسفين، وبالتالي، يكون هناك قدرة محوية أكبر لتنقل الكومة. بالإضافة إلى ذلك، قدرة التحمل للكومة يمكن تقليلها من خلال تقليل المسافة بين كومة وقمة المنحدر من الحركة الجانبية للتربة وتقليل وجود التربة على جانب الكومة. وبالإضافة على ذلك، فإن زيادة زاوية الميل يؤدي إلى زيادة النزوح الجانبي للكومة. ووجد بأن مركزية الحمولة المحورية للكومة تؤدي إلى انحناء أكثر للكومة وبالتالي زيادة الحد من القدرات المحورية. وتم عرض نتائج التحليل في شكل رسم بياني لعوامل التخفيض على الأحمال القصوى الأفقية.

Undrained vertical bearing capacity of pile located near soft clay slope

Mehrab Jesmani*, Ali Kasrania*, Mehrad Kamalzare** and Iman Mehdipour***

**Department of Civil Engineering, Imam Khomeini International University, Qazvin, Iran.*

*** Department of Civil and Environmental Engineering, Rensselaer Polytechnic Institute, Troy, NY; Adjunct Professor, Manhattan College, Riverdale, NY*

****Department of Civil Engineering, Missouri University of Science and Technology, Rolla, MO.*

***Corresponding author: Email: kamalmrpi@gmail.com.*

ABSTRACT

The bearing capacity of shallow foundations on slopes is commonly calculated from proposed design charts or using empirical equations. This paper presents the results of numerical studies carried out on behavior of pile located near soft clay slopes under undrained vertical loading conditions. A series of three-dimensional numerical models was performed for various pile geometry, different distances of the pile and slope angle. The obtained results show that, as the pile embedded length increases, full formations of wedge failure occurs and, therefore, a greater axial capacity of the pile is mobilized. In addition, by decreasing the distance of the pile from the slope crest, the lateral movement of soils increases and the lack of soils on the slope side of the pile tend to reduce the bearing capacity. Furthermore, by increasing the slope angle, the pile lateral displacement increases and, therefore, the eccentricity of the axial load on the pile will produce more additional bending moments in the pile and thereby the axial capacity reduction increases. The results of the analysis are presented in chart form as reduction factors (RF) on horizontal ground ultimate loads.

Keywords: Bearing capacity; pile; reduction factor; slope; three-dimensional analysis.

INTRODUCTION

When a footing is constructed on a sloping ground, the bearing capacity of the footing may be significantly reduced, depending on the location of the footing with respect to the slope. The bearing capacity of foundations on slopes is commonly calculated using empirical equations or from proposed design charts, which have been produced based on limit equilibrium or upper bound plasticity calculations. The lateral and axial behavior of pile foundations is different from those constructed on a level ground surface. Since full formations of shear zones under ultimate loading conditions are not possible on the sides close to the slopes or edges, the supporting capacity of soil on that side get considerably reduced. Under lateral loads, the piles not only may induce slope failure, particularly at shallow depths, but also may undergo severe reduction in its lateral capacity.

Poulos (1976) presented some results of an analysis of piles near slopes in clayey soils. It was reported that the deflection of a pile in a slope could be 1.6 times that of the same pile in horizontal ground surface. It was concluded that once the pile is greater than four pile diameters away from the crest of the slope, the slope has no effect on the ultimate capacity. Schmidt (1977) performed a series of laboratory model tests with rigid model piles to study the behavior of piles installed at the crests of four different sandy slopes. It was found that the horizontal ultimate capacity of vertical pile decrease as the slope became steeper. Bouafia & Bouguerra (1995) and Mezazigh & Levacher (1998) performed centrifuge tests to study the responses of piles in/near a slope under lateral loads. The results showed that, for a pile at the crest of a 1 (V) : 2 (H) slope, the lateral capacity and the maximum bending moment are approximately 0.70 and 1.25 times those for the reference pile in Horizontal ground surface. El Sawwaf (2006) and (2008) conducted a series of 36 small scale model tests on short rigid piles and intermediate length piles in sand slopes. The results of the tests showed that the load ratios (the ratio of the lateral capacity of the pile embedded in sloping ground to horizontal ground surface) of the pile immediately at the slope crest was 0.57. In addition, by polynomial interpolation, the load ratios for the pile located three pile diameters form the crest of the slope was predicted to be 0.93.

Chen & Martin (2001) conducted extensive Finite Element analyses of piles located near slope crests to evaluate the effects of slope and pile proximity to slope crest on the lateral resistance and p-y curves of the soil-pile system. Their results show that for slope angles less than 45º the effect of slope on ultimate load capacity becomes less than 10% for distances greater than 6 pile diameters, and therefore the slope effect beyond that can be neglected. Chae *et al.* 2004 performed several numerical studies with a three-dimensional finite element method of model tests and a prototype test of a laterally loaded short pile and pier foundation located near slopes, respectively. The main purpose of this paper is to point out that the three-dimensional elasto–plastic

FEM is very effective in the evaluation of the lateral resistance of a short pile and a real pier foundation placed near slopes. Georgiadis & Georgiadis (2010) performed three-dimensional finite element analyses to study the behavior of piles in sloping ground under undrained lateral loading conditions. The results indicated that, Pile-soil adhesion has an important effect on lateral pile behavior. Ziaie-Moayed *et al.* (2012) studied the behaviour of solid circular concrete piles in clayey soils under a combination of lateral and vertical loading using a numerical model. Piles with different lengths were considered, and ultimate lateral bearing capacity was calculated. The model was verified on the basis of data obtained from a previously published full scale pile load test. Particular attention was devoted to the influence of axial loading on lateral bearing capacity. A comparison was also performed between the results of FLAC 3D, ALLPILE and Broms approaches.

Other researchers investigated piles in different conditions (Ziai Moayed *et al.,* 2010); the behavior of piles under vertical loading near soft clay slopes is one of the interesting areas in geotechnical engineering. An increasing number of structures are constructed on soft clay ground, and the application of piles on soft ground is becoming an important issue in foundation design.

The bearing capacity of shallow foundations on slopes is commonly calculated from proposed design charts or using empirical equations (Jesmani & Kamalzare, 2010). It is clear that the axial capacity of pile located near a slope is smaller than that found for the same pile in horizontal ground surface. This is because of the lack of the soil mass on the slope side of the pile, which tends to reduce the pile bearing capacity. In this condition, full formations of shear zones under ultimate loading conditions are not possible on the side close to the slope, and the supporting capacity of soil on that side reduces significantly.

In this paper, three-dimensional finite element analyses were performed to study the effect of the lack of the soil on the behavior of piles in soft clay sloping ground under undrained vertical loading conditions. The varying parameters include the pile geometry, different distances of the pile from the slope and slope angle for pile subjected to vertical loading. The results of the analysis are presented in chart form as reduction factors (RF) on horizontal ground ultimate loads.

NUMERICAL SIMULATION AND CONSTITUTIVE MODELS

Finite element model

A finite element method is used to simulate the pile behavior described in this paper. The geometry of a three-dimensional model of a pile embedded in sloping ground is shown in Figure 1. Because of the symmetrical condition of the problem, only half of the pile section in the direction of the axial load is analyzed. The bottom elevation and

the lateral edges of the computational domain were taken far enough from the pile to avoid any significant boundary effect such as stress reflection (Jesmani *et al.,* 2013 and Jesmani *et al.,* 2011). For symmetry model, the width and length of soil mass are taken as $20B$ and $40B+H.\tan\alpha$ respectively (B is the pile width, α is the slope angle and H is the slope height). The height of soil mass is $L+20B$, in which, L is the embedded length of pile. The bottom boundary was fixed against movements in all directions, whereas the 'ground surface' was free to move in all directions. The vertical boundaries were fixed in the horizontal movements. A relatively fine mesh was used near the pile–soil interface, while a coarser mesh was used further from the pile (Jesmani *et al.,* 2014). The pile and the soil were modeled using 20-node quadrilateral brick elements with reduced integration.

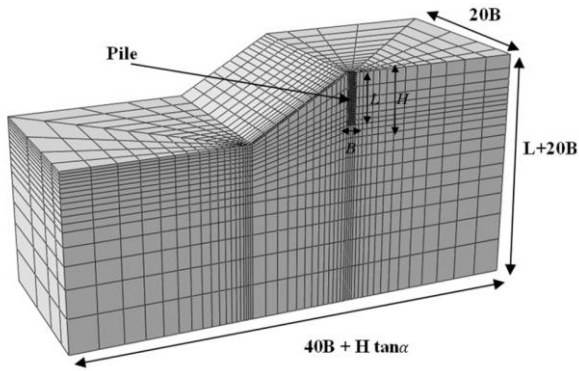

Fig. 1. Typical mesh for three-dimensional finite element analyses

In the analyses, the gravity load is first applied to the soil to establish the initial in situ stress states prior to the pile installation. The finite element analyses were carried out using the linear elastic model for the structure of the pile, while the Mohr-Coulomb model was used for representing the soil behavior surrounding the pile. The pile-soil interface elements give an effect on the behavior of a vertically loaded pile and the modeling of the pile–soil interfaces is an important concern. For the pile–soil interface, 2-D quadratic 18 node elements, which consisted of two 9 node surfaces compatible with the adjacent solid elements (the two surfaces coincide initially), were considered using Coulomb shear-strength criterion. The interface elements of zero thickness can only transfer shear forces across their surfaces when a compressive normal pressure acts on them. According to the German code DIN-4014 (1990) and Tomlinson (1994) the adhesion between pile and soil can be taken equal to the soil cohesion for soft clays. Therefore, in this study, the adhesion factor has given a value of one and has used zero frictional strength to represent undrained condition.

Validation of numerical model

The available experimental analyses on the behavior of piles under vertical loading on clayey soils are very limited. However, the literature shows that most published experimental reports have focused on the behavior of pile in sandy slopes under lateral loading. Therefore, in this verification, a pile located on slope under lateral loading was considered. Chae *et al.* 2004 conducted experimental tests on the model pile located near a 30° slope under lateral loading. The pile distance from the slope crest is 400 mm. The soil used in this small scale model tests was Onahama sand with a unit weight $\gamma = 15.68\ kN/m^3$ and friction angle $\phi = 47.5°$. The Young's modulus of the sand was 25.8 MPa with a Poisson ratio $\nu = 0.3$ and dilatation angel $\psi = 17.5°$. The model pile was made of smooth aluminum with a wall thickness of 3 mm and outside diameter of 100 mm. Pile was buried 500 mm deep in the ground for a constant embedment depth/ diameter ratio of 5.0 in the test. Lateral loads were applied to the pile head, which was 100 mm above the ground surface. In this verification, a slip element was used to represent the interface behavior between the pile and soil elements. The interface friction coefficient (μ) of 0.5 was adopted. Also, a limiting displacement of 5 mm was assumed for full mobilization of skin friction and also, providing convergence as suggested by Lee *et al.* 2002 . The comparative results of the experimental model and 3-D finite element analyses are shown in Figure 2. There is a good compatibility between the experimented results of published data and the present simulation model.

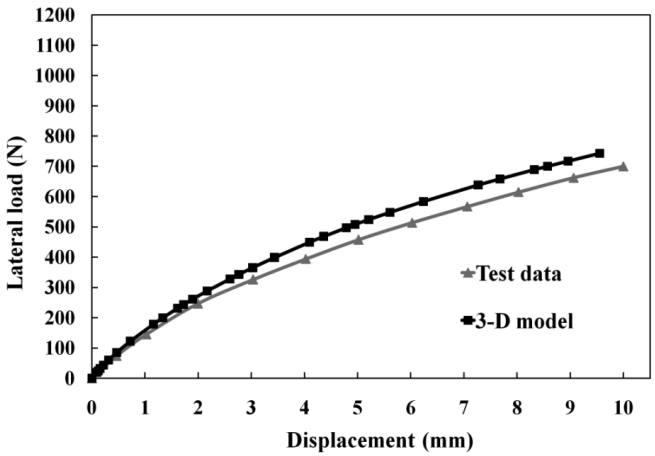

Fig. 2. Comparison of 3-D FEM results with experimental test result of Chae *et al.* 2004

Type of analysis

Soil and pile properties used in the finite element analyses are summarized in Table 1. It was tried to simulate the realistic soil properties corresponding to the field condition as soft clay soil.

Table 1. Soil and pile properties

Soil properties	Pile properties
Soil type: Soft clay	Density, γ = 23 (kN/m^3)
Bulk density, γ = 20 (kN/m^3)	Young's modulus, E = 2e+7 (kPa)
Poisson ratio, ν = 0.48	Cross section: Square
Undrained shear strength, c_u = 35 (kPa)	
Friction angle, ϕ = 0	
Young's modulus, E = 5e+3 (kPa)	

A series of numerical models was performed for various pile geometry, different distances of the pile from the slope crest and also slope angle. To simplify the representations of results, the dimensionless parameters L/H = embedded length ratio of the pile, L/B = ratio of pile length to pile width and X/B = distance ratio of the pile from the slope are used. These parameter have been illustrated in Figure 1. The schematic of the model analyzed is illustrated in Figure 3. The bearing capacity of shallow foundations on or near slopes is commonly calculated from proposed design charts. So, in the present paper, similar to the shallow foundations, this decrease is normally defined in a non-dimensional form, RF, called the axial capacity reduction factor of pile and defined by:

$$RF = \frac{Q_{ps}}{Q_{ph}} \tag{1}$$

where Q_{ps} and Q_{ph} are the axial capacity of the pile embedded in sloping ground and horizontal ground surface, at the same settlement respectively. It should be noted that, in all analyses the height of the slope is lower than 8 m which were corresponded to safety factors greater than 1.2.

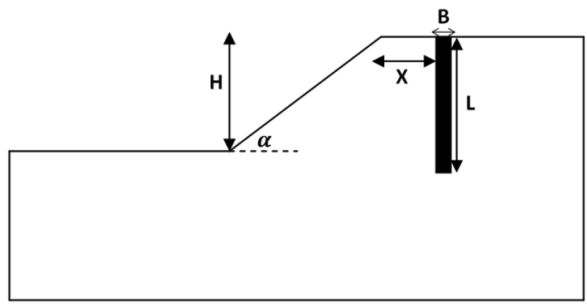

Fig. 3. Schematic view of the model

RESULTS AND DISCUSSION

Load-settlement behavior

Some of the load-settlement behaviors resulted from the finite element analyses for different length ratio (L/H), distance ratio (X/B) and slope angles α = 30° and 60° are presented as an example in Figure 4. It is clear that the axial capacity of pile located near a slope is smaller than that found for the same pile in horizontal ground surface. Full formations of shear zones under ultimate loading conditions are not possible on the side close to the slope, and so, the supporting capacity of soil on that side gets considerably reduced. As expected, due to the soil properties as soft clay, the shearing stress increases with increasing displacement until yield occurs and then remains constant. In Figure 4, the load-settlement curves have three distinct slope angles. Initial slope of the load settlement curve is stiffer due to the load carrying capacity of the shaft and base of the pile. However, in this part the load carrying capacity of the pile is mainly borne by the shaft. By increasing the vertical load on the top of the pile the ultimate skin resistance would be achieved and the additional load imposed is essentially carried on the base of the pile. In this stage, a significant change in the slope of the load-settlement curves takes place that means the soil stiffness considerably decreases. Finally, in the third region, the load-settlement curves take practically a horizontal linear form that is called failure region and, therefore, the ultimate vertical bearing capacity of pile can be determined. In this region, both ultimate skin resistance and base resistance of the pile have been achieved.

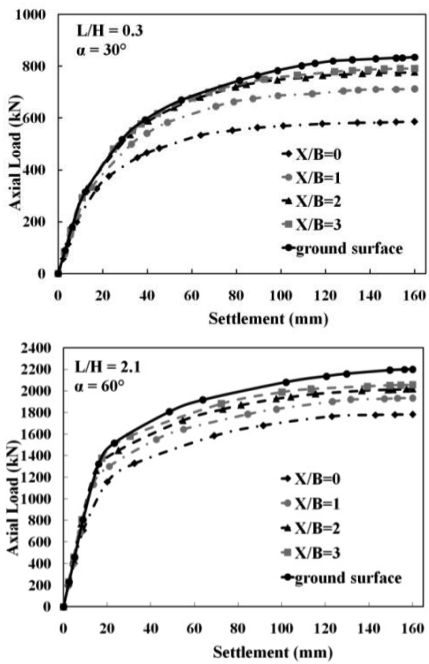

Fig. 4. Load-settlement curves for slope angle $\alpha = 30°$ and $\alpha = 60°$

The obtained results show that, the effect of sloping ground on the ultimate capacity of pile seems to be more dominant as the ratio of pile length to slope height (L/H) decreases. For example, for the L/H = 0.3, X/B = 0 and $\alpha = 30°$, the ultimate axial capacity is 30% lower than that for level ground. On the other hand, for the L/H = 2.1 and the same distance ratio and slope angle, this decrease in ultimate axial capacity becomes 15%. This can be due to the fact that, as the pile embedded length increases, full formations of wedge failure under ultimate loading conditions occurs, and therefore, a greater axial bearing capacity of the pile is mobilized. Similar behavior is observed in the load-settlement response for slope angle $\alpha = 60°$. Moreover, by increasing the slope angle, the ultimate axial capacity considerably decreases. For example, for the L/H = 0.3, X/B = 0 and $\alpha = 30°$, the ultimate axial capacity is 30% lower than that for level ground. But, for the $\alpha = 60°$ and the same conditions, this decrease becomes 44%. In addition, at the same bearing pressure, by increasing the slope angle from $\alpha = 30°$ to 60°, the settlement of the pile increases. Figure 4 shows that, by increasing the pile distance from the crest of slope, the ultimate axial capacity increased. Therefore, by increasing the distance ratio of the pile from the slope, the effect of slope on the ultimate capacity of pile decreases. The shear strain distribution patterns for skin and below of the pile for different cases are calculated. Figure 5 shows the shear strain distribution below the pile for the case with $\alpha = 30°$, L/H = 2.1, and X/B = 0 as an example.

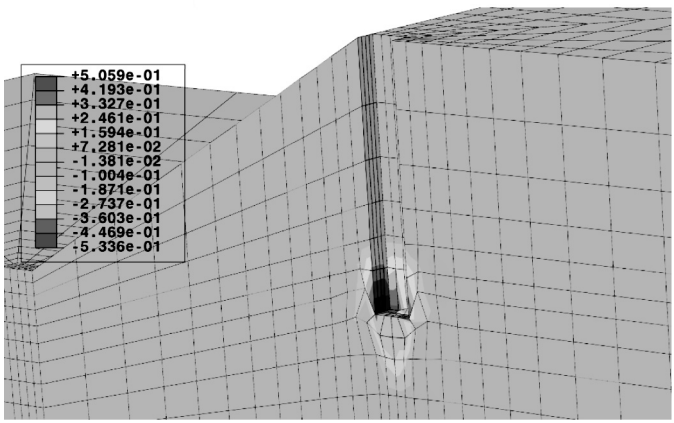

Fig. 5. Shear strain distribution below the pile ($\alpha = 30°$, L/H = 2.1, and X/B = 0)

Variation of reduction factor with pile settlement

The variation of reduction factor (RF) versus pile settlement ratio (S/B) for some of the slope angles is presented in Figure 6, where *S* is the pile settlement. It should be noted that for each case the axial load for a pile near the slope is normalized by the load in the horizontal ground case at the same settlement. The obtained results show

that, the reduction factor in any case depends on the embedded length of the pile, the distance of the pile from the crest of the slope and the slope angle. It can be clearly seen that, the reduction factor increased with the increasing distance ratio, and also RF decreased as the length ratio of pile decreased.

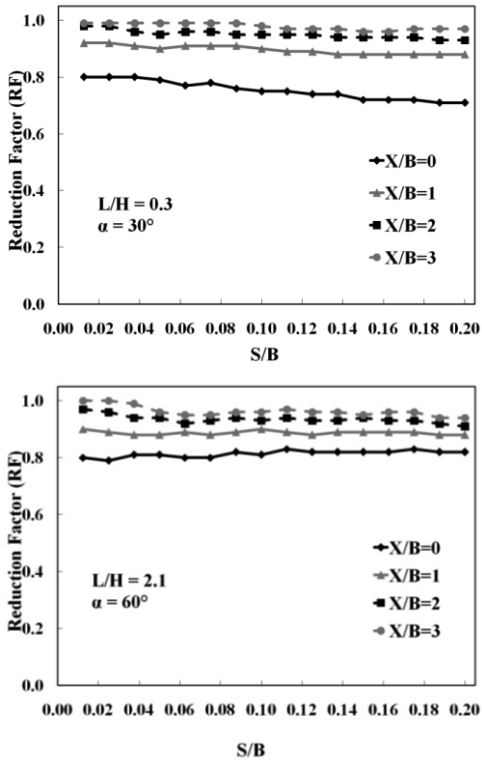

Fig. 6. Variation of reduction factor with pile settlement for slope angle $\alpha = 30°$ and $\alpha = 60°$

The bearing capacity of foundations on or near slopes is commonly calculated using empirical equations or from design charts. For example, Meyerhof (1957) proposed design charts which are currently adopted by many design manuals such as Unified Facilities Criteria (UFC) and WSDOT 2005 Geotechnical Design Manuals. Castelli & Motta (2008) have used the method of slices to propose design charts for drained and undrained slopes. Therefore, in this paper, the variation of reduction factor with embedded length ratio (L/H) of the pile, distance ratio of the pile from the slope (X/B) and slope angles are shown as design charts.

Table 2 shows the maximum, minimum and average values of reduction factor for each pile settlement to pile width ratio (S/B). As can be seen, by increasing the embedded length of the pile and the distance ratio of the pile from the slope, the variation of Δ(RF) decreased. The standard deviation (SD) and coefficient of variation (COV) for each set of data (load-settlement) are also calculated. COV is defined as

the ratio of the standard deviation to the average of RF for each set of load-settlement data. Based on the results the COV of data for all load-settlement curves were less than 0.07 for the numerical analyses. Consequently, in this paper the average of reduction factor for each load-settlement data considered correspond to ultimate axial capacity reduction factor. Variation of reduction factor with embedded length ratio (L/H) of the pile, pile length to pile width ratio (L/B), distance ratio of the pile from the slope (X/B) and slope angles are discussed in details in the following section.

Table 2. Variation of reduction factor

α		30°						60°					
L/H		0.3	0.9	1.5	2.1	3.3	5.0	0.3	0.9	1.5	2.1	3.3	5.0
X/B = 0	$(RF)_{min}$	0.71	0.79	0.83	0.86	0.89	0.93	0.57	0.67	0.76	0.79	0.87	0.90
	$(RF)_{ave}$	0.76	0.82	0.86	0.88	0.93	0.97	0.62	0.71	0.78	0.81	0.89	0.95
	$(RF)_{max}$	0.80	0.86	0.87	0.89	0.95	1	0.68	0.75	0.80	0.82	0.92	0.98
	SD	0.03	0.03	0.01	0.01	0.02	0.02	0.04	0.03	0.01	0.01	0.01	0.02
	COV	0.04	0.03	0.02	0.01	0.02	0.03	0.07	0.04	0.02	0.02	0.02	0.02
X/B = 1	$(RF)_{min}$	0.88	0.88	0.89	0.92	0.95	0.96	0.78	0.79	0.86	0.88	0.89	0.93
	$(RF)_{ave}$	0.89	0.9	0.92	0.94	0.98	1	0.82	0.84	0.88	0.89	0.93	0.97
	$(RF)_{max}$	0.92	0.92	0.92	0.95	1	1	0.84	0.86	0.89	0.9	0.95	1
	SD	0.02	0.03	0.01	0.01	0.01	0.01	0.02	0.02	0.01	0.01	0.01	0.01
	COV	0.02	0.03	0.02	0.01	0.02	0.02	0.02	0.03	0.01	0.01	0.02	0.02
X/B = 2	$(RF)_{min}$	0.92	0.92	0.92	0.95	0.95	0.97	0.88	0.88	0.89	0.91	0.94	0.97
	$(RF)_{ave}$	0.94	0.95	0.95	0.96	0.99	1	0.90	0.91	0.93	0.94	0.97	0.99
	$(RF)_{max}$	0.97	0.98	0.98	0.98	1	1	0.95	0.95	0.95	0.97	1	1
	SD	0.01	0.02	0.01	0.01	0.01	0.01	0.02	0.02	0.02	0.01	0.01	0.01
	COV	0.02	0.02	0.02	0.01	0.01	0.01	0.02	0.02	0.02	0.02	0.01	0.01
X/B = 3	$(RF)_{min}$	0.95	0.95	0.96	0.96	0.98	1	0.92	0.92	0.93	0.94	0.96	0.99
	$(RF)_{ave}$	0.97	0.97	0.98	0.98	1	1	0.95	0.95	0.96	0.97	1	1
	$(RF)_{max}$	0.99	0.99	0.99	1	1	1	0.97	0.97	0.99	1	1	1
	SD	0.01	0.01	0.01	0.01	0.01	0	0.01	0.02	0.02	0.02	0.01	0.01
	COV	0.01	0.01	0.01	0.01	0.01	0	0.01	0.02	0.02	0.02	0.02	0.01
X/B = 4	$(RF)_{min}$	1	1	1	1	1	1	1	1	1	1	1	1
	$(RF)_{ave}$	1	1	1	1	1	1	1	1	1	1	1	1
	$(RF)_{max}$	1	1	1	1	1	1	1	1	1	1	1	1
	SD	0	0	0	0	0	0	0	0	0	0	0	0
	COV	0	0	0	0	0	0	0	0	0	0	0	0
$\Delta(RF_{min})$		0.27	0.19	0.15	0.13	0.1	0.07	0.39	0.29	0.21	0.18	0.1	0.1
$\Delta(RF_{ave})$		0.24	0.18	0.14	0.12	0.07	0.03	0.36	0.27	0.22	0.19	0.11	0.05
$\Delta(RF_{max})$		0.2	0.14	0.13	0.11	0.05	0	0.32	0.25	0.2	0.18	0.08	0.02

Effect of pile geometry

Figures 7(a) and (b) show the variation of reduction factor against normalized pile length L/H for different slope angles. It is clear that the pile performance improves much with the increase of pile embedded length. This can be due to the fact that, as the pile embedded length increases, the full formations of wedge failure under ultimate loading conditions occurs and also the effect of the lack of soil on the slope side of the pile decreases. This means that a longer failure surface develops, the failure wedge becomes larger and hence a greater axial bearing load capacity of the pile is mobilized. Moreover, by increasing the length of the pile, the length of adhesion between soil and pile increase. In addition, the numerical results show that, as the pile approaches failure, the vertical settlements are accompanied by horizontal movements and rotations toward the slope. When the pile moves laterally, the eccentricity of the axial load on the pile will produce additional bending moments in the pile and thereby reduce the axial capacity. The existence of pile can also decrease the lateral deformations of soil particles. Therefore, as the pile length increases, the resistance of pile to the lateral movement of soil particles increase and, so, the axial bearing capacity of pile improves.

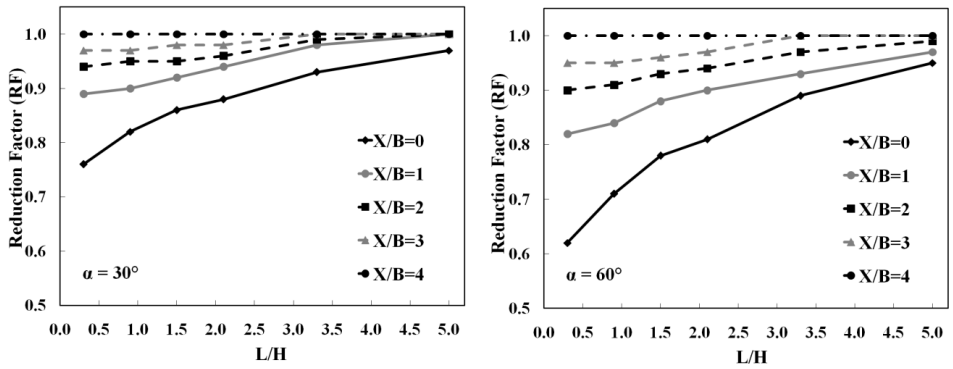

Fig. 7. Variation of reduction factor with pile embedded length for slope angle (a) $\alpha = 30°$ and (b) $\alpha = 60°$

Figure 8 presents the lateral deformation of soil particles against normalized slope elevation (z/H) for a pile placed at the crest for pile length L/H = 0.9 and L/H = 1.5, respectively. The Figure clearly shows as the length of pile decreases, the horizontal movement of soil particles increases to the outside region and, hence, the slope deformation also increases. The lateral displacement vectors of soil particles for the case with L/H = 0.9 is shown in Figure 9.

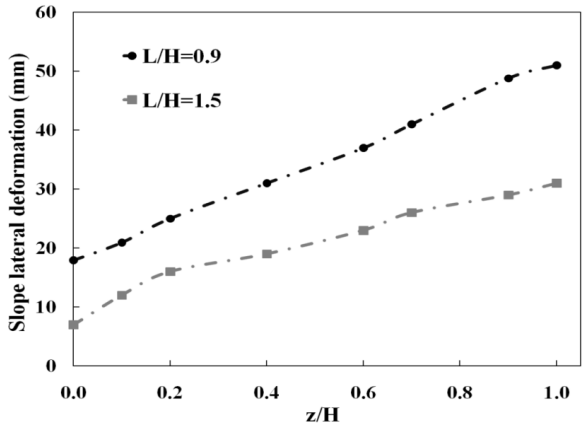

Fig. 8. Influence of pile length on slope lateral deformation

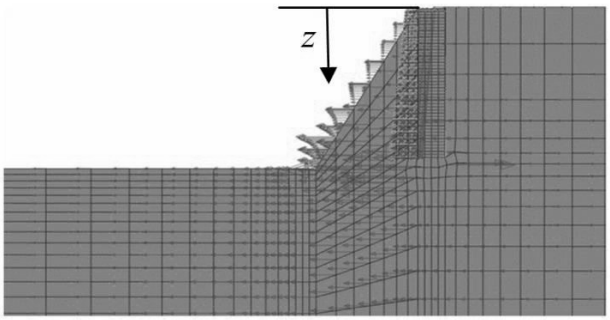

Fig. 9. Lateral displacement vectors of soil particles of slope L/H = 0.9

Figure 10 shows the variation of different pile length to pile width (L/B) for different slope angles. When the pile length is much greater than the slope height, the greater length of pile is not affected by the slope. This means that a longer failure surface develops, the failure wedge becomes larger and hence a greater axial bearing load capacity of the pile is mobilized. Moreover, by decreasing the pile width (B), the failure wedge becomes small and so, the possibility of full formations of wedge failure increases and the effect of the lack of soils on the slope side of the pile decreases. Therefore, by increasing the pile length or decreasing the pile width, the effect of slope on pile bearing capacity reduction decreases.

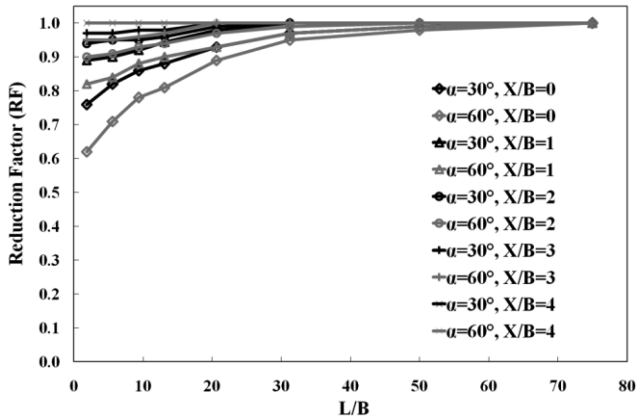

Fig. **10**. Variation of reduction factor to pile geometry

The obtained results show that, the degrees of improvement varied depending on the slope angle and the distance of the pile from the crest of the slope. These results are discussed in the following sections.

Effect of pile distance from slope crest

The relationship between reduction factor and distance of the pile from the crest of the slope for different embedded length ratio (L/H) and slope angles are shown in Figure 11(a) and (b). The obtained results show that the reduction factor increases significantly as the pile moves away from the crest of the slope. This can be explained by the fact that, as the pile is installed far from the crest of the slope, the effect of the lack of soils on the slope side of the pile decreases, the failure wedge becomes larger and, therefore, the total shear force increases. In general, the same trend is observed for different pile depth and slope angles. But, when the pile is placed directly at the crest (X/B= 0), increasing the embedded length of pile leads to significant increase in the reduction factor. For slope angles $\alpha = 30°$ and 60° the values of reduction factor are approximately 0.98 and 0.96 respectively, when the pile is located at a distance equal to 3B from the crest of the slope. Even in this case, the difference between the horizontal ground and the slope condition is clear. However, this increase in the reduction factor is obvious until a value of about X/B = 4 after which the effect of slope can be neglected and the reduction factor approaches to one (i.e. $RF \rightarrow 1$). Therefore, it can be concluded that, to obtain a load ratio = 1.0 (equivalent to the horizontal ground condition), it may be necessary to move the pile to a distance larger than 4B from the crest of the slope. This ratio of X/B after which the slope has no effect on the pile is consistent with the value obtained by Poulos (1976),; Chae *et al.* 2004 and El Sawwaf (2006) and (2008).

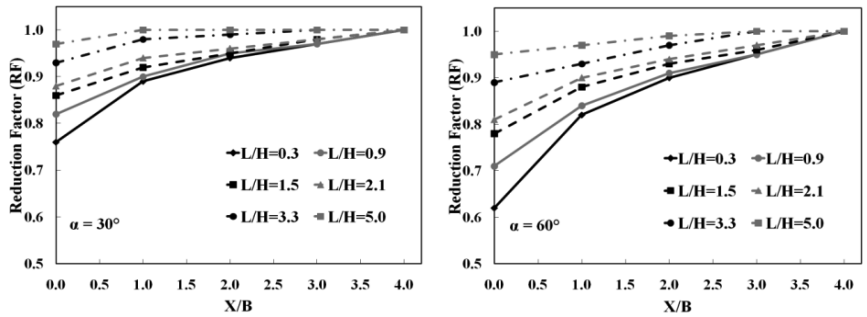

Fig.11. Reduction factor versus distance of the pile from the slope crest for (a) $\alpha = 30°$ and (b) $\alpha = 60°$

Effect of slope angle

Figure 12 shows the variation of reduction factor for different slope angles. It is clear that, increasing the slope angle decreased the reduction factor of pile in sloping ground. For example, for the L/H = 0.9, X/B = 0 and $\alpha = 30°$, the ultimate axial capacity is 28% less than that for level ground. For $\alpha = 60°$ and the same conditions, this decrease becomes 36%. This is due to the fact that, by increasing the slope angle, the lateral deformation of soil particles around the pile increases and, hence, the axial bearing capacity decreases. This observation of the pile in a slope is consistent with the conclusion given by Azzam & Nazer (2010).

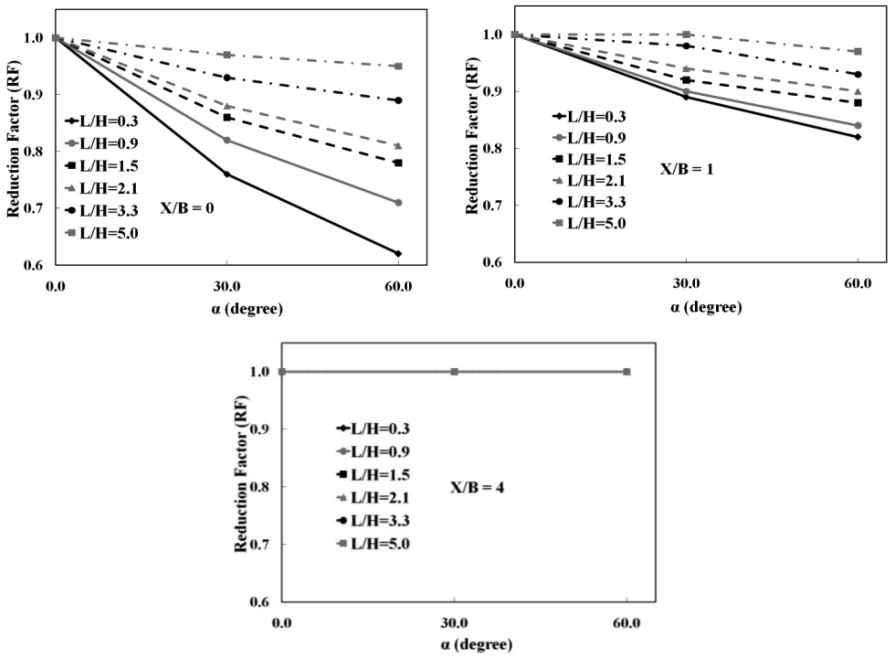

Fig. 12. Variation of reduction factor with slope angles for different pile distance from the slope crest

In addition, by increasing the slope angle, pile lateral displacement increases and, thus, the eccentricity of the axial load on the pile will produce more additional bending moments in the pile. Therefore the axial capacity reduction increases. Figure 13 presents pile lateral displacement along the normalized pile elevation (z/L) for a pile placed at the crest for pile length L/H = 0.9 and different slope angles. It can be seen that, by increasing the slope angle, the pile lateral displacement increases and so, eccentricity of the axial load on the pile is increased. As an example, the effect of slope angle on the lateral displacement vectors of soil particles for L/H = 0.9, and α = 60° is shown in Figure 14.

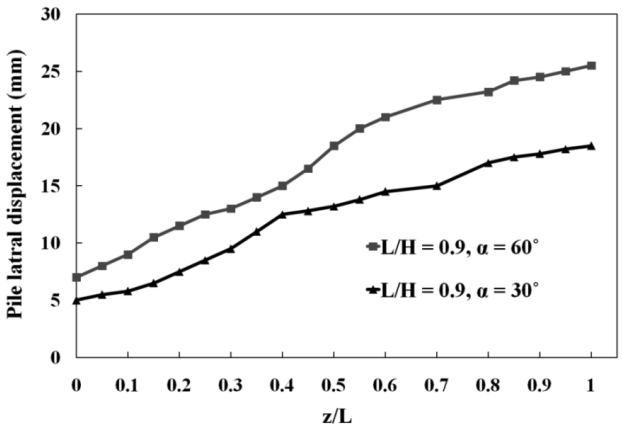

Fig. 13. Influence of slope angle on the variation of pile lateral displacement

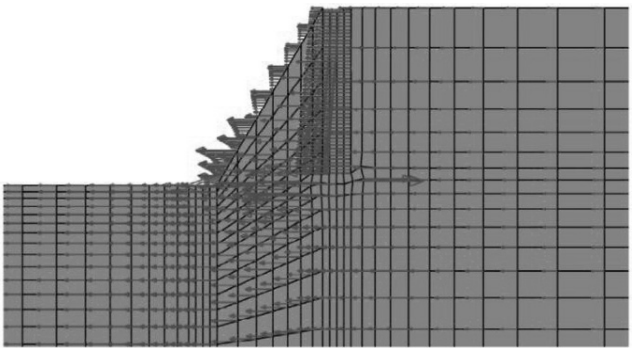

Fig. 14. Influence of slope angle on the lateral displacement vectors of soil particles for L/H = 0.9, and $\alpha = 60°$

The results show that by increasing the embedded length of the pile and pile distance from the slope crest, the effect of the slope angle on the reduction factor of the pile axial capacity decreases. For instance, for the L/H = 2.1, X/B = 0, and $\alpha = 60°$ the ultimate axial capacity is 6% less than the case with $\alpha = 30°$.

CONCLUSIONS

The purpose of this paper is to study the behavior of piles on soft clay sloping ground under undrained vertical loading conditions. A series of 3-D numerical models was performed for various pile geometry, different distances of the pile from the slope and slope angle. It should be noted that, in all analyses the height of the slope is lower than 8 m. The conclusions obtained from this study are summarized as follows:

1. The reduction factor (RF) in any case depends on the pile geometry, the distance of the pile from the crest of the slope and the slope angle.
2. The effect of sloping ground on the ultimate capacity of pile seems to be more dominant as the length of the pile decreases. For instance, for the L/H = 2.1, X/B = 0, and slope angle $\alpha = 60°$ the ultimate axial capacity is 6% less than the case with slope angle $\alpha = 30°$.
3. Pile performance improves much with the increase in ratio of pile embedded length to pile width. This can be due to the fact that, as the pile embedded length increases, the full formations of wedge failure under ultimate loading conditions occurs and, so, the failure wedge becomes larger. Moreover, by decreasing the pile width, the failure wedge becomes small and so, the possibility of full formations of wedge failure increases.
4. The reduction factor increases significantly as the pile moves away from the crest of the slope. This can be up to 25% and 35% for the slope angles α = 30° and 60° respectively. Besides, by increasing the pile distance from the slope, the effect of the lack of soils on the slope side of the pile and the lateral movement of soils decrease.
5. By increasing the slope angle, the lateral deformation of soil particles around the pile increases and, hence, the axial bearing capacity decreases. By increasing, the pile lateral displacement, the eccentricity of the axial load on the pile will produce more additional bending moments in the pile and so the axial capacity reduction increases.
6. The influence of the slope ground on the pile axial capacity can be neglected once the pile is placed at a distance of more than 4B from the crest of the slope (i.e. $RF \rightarrow 1$). This ratio of X/B after which the slope has no effect on the pile is consistent with the value obtained by Poulos (1976); Chae *et al.* 2004 and El Sawwaf (2006) and (2008).

REFERENCES

Azzam, W. & Nazer, A. 2010. Improving the bearing capacity of footing on soft clay with sand pile with/ without skirts, International Review of Civil Engineering Journal. Vol. **1**, No. 1, pp. 32-38.

Bouafia, A. & Bouguerra, A. 1995. Centrifuge testing of the behavior of a horizontally loaded flexible pile near to a slope. Canadian Geotechnical Journal, **32**(2), 324-335.

Castelli, F. & Motta, E. 2008. Bearing capacity of shallow foundations near slopes: Static analysis. Proceedings of the 2nd BGA International Conference on Foundations, ICOF 2008, HIS BRE Press, Watford, U.K., 1651-1660.

Chae, K. &, Ugai, K. & Wakai, A. 2004. Lateral resistance of short single piles and pile groups located near slopes. International Journa of Geomechanics, **4**(2), 93-103.

Chen, C.Y. & Martin, G.R. 2001. Effect of embankment slope on lateral response of piles. Proceedings of the International Conference on FLAC and Numerical Modeling in Geomechanics, Lyon, France, pp. 47-54.

DIN-4014. 1990. Bored piles: Construction procedure, Design and bearing behaviour. Berlin, German code.

El Sawwaf, M. 2008. Lateral behavior of vertical pile group embedded in stabilized earth slope. Journal of Geotechnical and Geoenvironmental Engineering, **134**(7), 1015-1020.

El Sawwaf, M. 2006. Lateral resistance of single pile located near geosynthetic reinforced slope. Journal of Geotechnical and Geoenvironmental Engineering, **132**(10), 1336-1345.

Georgiadis, K. & Georgiadis, M. 2010. Undrained lateral pile response in sloping ground. Journal of Geotechnical and Geoenvironmental Engineering, **123**(11), 1489-1500.

Jesmani, M. . &, Nabavi, S. H. & Kamalzare, M. 2014. Numerical analysis of buckling behavior of concrete piles under axial load embedded in sand. Arabian journal of science and engineering, Vol. **39** (4), pp. 2683-2693.

Jesmani, M. & , Kamalzare, M. & Nazari, M. 2013. Numerical study of behavior of anchor plates in clayey soils. International Journal of Geomechanics, ASCE, Vol. **13** (5), pp. 502-513.

Jesmani, M. &, Hamissi, A. &, Kamalzare, M., & Vileh, R. S. 2011. Optimum geometrical properties of active isolation. Proceedings of the ICE - Geotechnical Engineering, Vol. **164**, (6), pp: 385-400.

Jesmani, M. & Kamalzare, M. 2010. Comparison between numerical and analytical solutions of dynamic response of circular shallow footing. Electronic Journal of Geotechnical Engineering; Vol. 15/P.

Lee, C.J. & Bolton, M.D. & Al-Tabbaa, A. 2002. Numerical modelling of group effects on the distribution of drag loads in pile foundations. Geotechnique, **52**(5):325–35.

Meyerhof, G. G. 1957. The ultimate bearing capacity of foundations on slopes. Proceedings of the 4th International Conference on Soil Mechanics and Foundation Engineering, London, UK, Vol. 1, pp. 384-386.

Mezazigh, S. & Levacher, D. 1998. Laterally loaded piles in sand: Slope effect on p-y reaction curves. Canadian Geotechnical Journal, **35**, 433-441.

Poulos, H.G. 1976. Behavior of laterally loaded piles near a cut or slope. Australian Geomechanics Journal **6**(1), 6-12.

Schmidt, H. G. 1977. Large diameter bored piles for abutments. Proceedings of the 9th International Conference on Soil Mechanics and Foundation Engineering, Tokyo, Japan, 107–112.

Tomlinson, M. J 1994. Pile design and construction practice. E&FN Spon: London.

WSDOT, 2005. Geotechnical design manual M46-03, Washington State Department of Transportation, Washington, USA.

Ziai Moayed, R., Kamalzare, M. & Judi, A. 2012. Three dimensional analyses of concrete piles in clayey soils. Proceedings of the ICE - Geotechnical Engineering, Vol. **166** (4), pp. 399- 407.

Ziai Moayed, R. , Kamalzare, M. & Safavian, M. 2010. Evaluation of piled raft foundations behavior with different dimensions of piles. Journal of Applied Sciences, Vol. **10** (13), pp. 1320-1325.

Submitted: 21-09-2014
Revised: 16-04-2015
Accepted: 29-04-2015